Adsorption of a Benzylic Amide Macrocycle on a Solid Substrate: XPS and HREELS Characterization of Thin Films Grown on Au(111)

Caroline M. Whelan,[†,‡] Francesca Cecchet,[†] Richard Baxter,[§,⊥] Francesco Zerbetto,*[,‡] Guy J. Clarkson,[||] David A. Leigh,[||] and Petra Rudolf*[,†]

Laboratoire Interdisciplinaire de Spectroscopie Electronique, Facultés Universitaires Notre-Dame de la Paix, 61 Rue de Bruxelles, B-5000 Namur, Belgium, Dipartimento di Chimica "G. Ciamician", Università degli Studi di Bologna, V. F. Selmi 2, 40126 Bologna, Italy, and Centre for Supramolecular and Macromolecular Chemistry, Department of Chemistry, University of Warwick, Coventry CV4 7AL, U.K.

Received: February 5, 2002

Thin films of a benzylic amide macrocycle, the common component of a wide class of mechanically interlocked molecules, are prepared by vapor deposition on Au(111). The films are characterized by monochromated X-ray photoelectron spectroscopy (XPS) and high resolution electron energy loss spectroscopy (HREELS). The relative amounts of carbon, nitrogen, and oxygen are consistent with the formation of intact molecular species. At monolayer coverage, the relative intensity of out-of-plane to in-plane phenyl ring vibrational modes indicates that the macrocycle adopts a nearly flat-lying conformation. The formation of a chemisorption bond is evidenced by the presence of a Au−O stretching vibration and a low binding energy component in the O 1s core level region assigned to interfacial bonding. A decrease in film order and the absence of a preferred molecular orientation is observed at higher coverages. Computer modeling of the adsorption of the macrocycle on the surface rationalizes the experimental observations.

1. Introduction

Molecular versions of some of the fundamental components of machinery from the macroscopic world, e.g., "shuttles",[1−5] "brakes",[6] "ratchets",[7,8] "turnstiles",[9] unidirectional spinning "motors",[10,11] etc., are currently being targeted as prototypical structural units for devices that could work through mechanical motion at the molecular level.[12−16] A common design feature behind many of these structures is that the molecular architectures are chosen so as to restrict the degrees of freedom of movement of submolecular components which, ideally, can then only move with respect to each other via discrete, large amplitude, internal motions. Mechanically interlocked structures, in the form of catenanes, consisting of two or more interlinked rings, and rotaxanes, where one or more macrocycles are locked onto a linear "thread" by bulky "stoppers", see Figure 1, are particularly interesting in this regard because the mechanical, as opposed to chemical, bond between the components allows their relative dynamics to be controlled through local environmental and external stimuli.[17] A further unique feature of these architectures is that translational (shuttling) or rotational (pirouetting) movement of the mechanically interlocked components can selectively hide or reveal a particular functionality or change the interactions between pendant groups on the macrocycle and thread. In essence, changing the location of a macrocycle between two or more inequivalent sites, i.e., the existence of translational or positional isomerism, promises the switching of macroscopic material properties through controlled motion at the molecular level.[1−5,14,15,17]

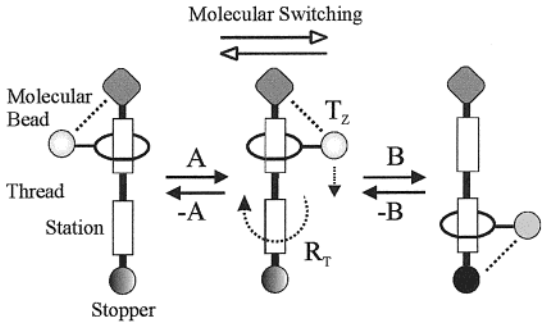

Figure 1. Schematic diagram of the mechanically interlocking components of a rotaxane comprising a thread and bead assembly showing restricted isomerism along the rotational (R_Z) and translational (T_Z) axes switched by environmental or external stimuli (A and B).

As a starting point in the effort to make catenanes and rotaxanes a technological reality, we have studied the interaction of the prototypical benzylic amide macrocycle (Figure 2a) with the Au(111) surface using X-ray photoelectron spectroscopy (XPS) and high resolution electron energy loss spectroscopy (HREELS). The measurements are supported by computer simulations which address the interaction between the macrocycle and the Au surface at the microscopic level. While the macrocycle itself has no possibility to exhibit translational isomerism, it is nonetheless a basic building block in a class of catenanes and rotaxanes (Figure 2b, for example) and hence unraveling its bonding and structure on a solid substrate may provide further insight into the design and assembly of more complex functional layers.

2. Experimental Section

The Au single crystal (10 × 7 × 2 mm) oriented to within 0.5° of the (111) plane (Metal Crystals and Oxides) was cleaned

* Corresponding authors. For experiments, contact Petra Rudolf. E-mail: petra.rudolf@fundp.ac.be. For calculations, contact Francesco Zerbetto. E-mail: gatto@ciam.unibo.it.

† Laboratoire Interdisciplinaire de Spectroscopie Electronique.

‡ Current address: Interuniversity Microelectronics Center, Kapeldreef 75, B-3001 Leuven, Belgium.

§ Dipartimento di Chimica "G. Ciamician".

|| Centre for Supramolecular and Macromolecular Chemistry.

⊥ Department of Materials, University of Oxford, Parks Road, Oxford OX1 3PH, U.K.

10.1021/jp020338a CCC: $22.00
Published on Web 07/31/2002

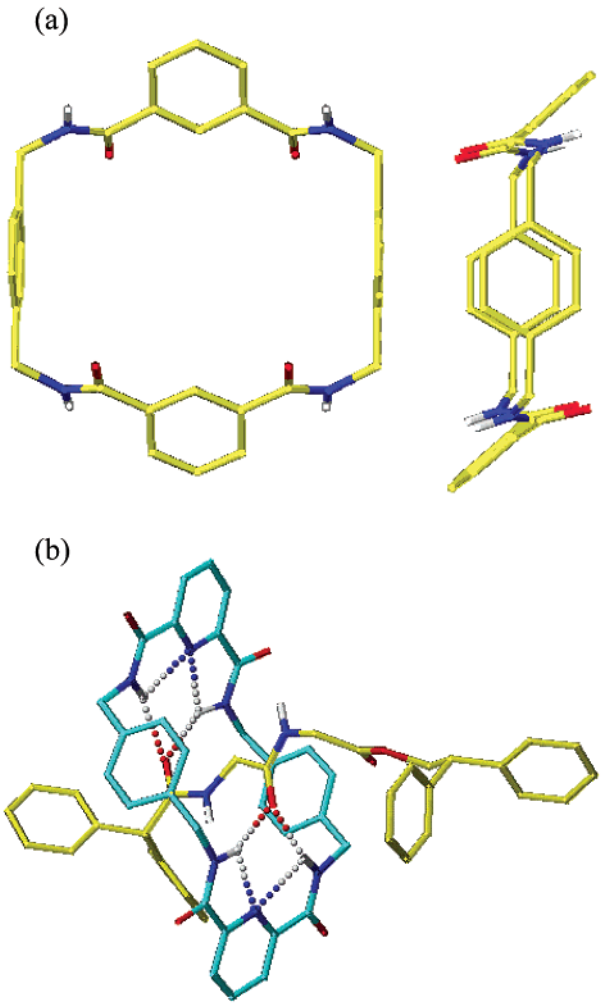

Figure 2. X-ray crystal structure of (a) benzylic amide macrocycle (including a side view) and (b) a glycylglycine [2]rotaxane. Color code: carbon = yellow/cyan, nitrogen = blue, oxygen = red.

in situ by cycles of argon ion bombardment (0.5 kV, 15 mA) and annealing to ~800 K followed by low energy electron diffraction, HREELS, and XPS confirmation of the surface crystallography and cleanliness. Synthesis of the benzylic amide macrocycle (1,7,14,20-tetraaza-2,6,15,19-tetraoxo-3,5,9,12,16,-18,22,25-tetrabenzocyclohexosane), the X-ray crystal structure of which is shown schematically in Figure 2a, is described elsewhere.[18,19] Thin films were prepared by in situ sublimation of the macrocycle on Au(111) at 300 K using a custom built cell consisting of a Pyrex crucible heated resistively to 530 K with the temperature being measured by a chromel−alumel junction fixed at the tube exit. Exposures were monitored using an uncalibrated Bayard−Alpert ionization gauge. All macrocycle dosing and sample annealing was performed in the preparation chambers to prevent contamination of the spectrometer vessels. In the XPS experiments, the coverage (defined in terms of a physical monolayer = 1 ML) was estimated by comparing the C 1s to Au $4f_{7/2}$ ratio with that measured from a film of known carbon atomic density (as outlined in section 4.1).[20] In the case of the vibrational measurements, the characteristic monolayer spectrum was identified by annealing a multilayer sample leaving only the chemisorbed monolayer on the surface. With this reference, spectra corresponding to less than or more than a physical monolayer can be identified with confidence.

HREELS data was collected with a Riber Sedra spectrometer equipped with sample preparation and main analyzer chambers operated at base pressures in the low 10^{-9} and 10^{-10} Torr range, respectively. The analysis chamber consisted of a 180° hemispherical monochromator and analyzer ensemble described in more detail elsewhere.[21] HREELS spectra were recorded with an incident beam energy of 6.0 eV (E_p) and collected both in specular ($\theta_i = \theta_r = 45°$) and off-specular ($\theta_i = 45°$, $\theta_r = 25°$) scattering geometries. The spectra presented here are normalized to the specular elastic peak intensity. The instrumental resolution, defined by the full-width-at-half-maximum (fwhm) of the elastic peak, varied between 10 and 21 meV for these measurements.

High-resolution XPS measurements were performed with a Scienta ESCA 300 photoelectron spectrometer (operated at base pressures in the low 10^{-10} Torr range) using a monochromated Al Kα ($h\nu = 1486.6$ eV) rotating anode X-ray source operated at 16 kV and 400 mA. Photoelectrons were detected by a hemispherical analyzer and a two-dimensional position-sensitive detector (microchannel plates with CCD camera). Different combinations of pass energy and exit slit-aperture width of the analyzer allowed variation of the energy resolution which was set at 0.45 eV for the C1s, O1s, and N1s core level spectra reported here. The photoelectron takeoff angle was 90°. All binding energies were referenced to the Au $4f_{7/2}$ core level.[22]

3. Computational Section

Modeling of an organic molecule on a gold surface requires to account for intramolecular interactions, gold−gold interactions, and gold−adsorbate interactions. Benzylic amide derivatives have been successfully simulated[23−25] by the MM3 model[26−28] implemented in the Tinker package.[29−31] The Ercolessi potential was used to simulate the gold substrate.[32] Finally, the gold−adsorbate interactions were considered using a combination of repulsive and Coulombic terms. The Coulomb charges were calculated using the charge equilibration, QEq, method developed by Rappe and Goddard[33] which is capable of calculating the charges on all the atoms within the system from the electronegativity of the individual atoms. The repulsive term was a Born−Mayer potential that was applied between each atom of the macrocycle and the gold atoms of the surface. The advantage of this approach is that no preset Au−macrocycle bonds had to be established from the "outside" and, in the calculations, the macrocycle was free to move on the surface, choosing its optimum position, without predefined constraints.

More detailed, the QEq scheme assumes that the electronegativity of an atom depends on its "intrinsic" electronegativity and a term which varies as a function of charge of the site: as an atom becomes more negatively charged, its electronegativity decreases. The charge distribution within the system is calculated by solving a series of coupled equations, which consider the intrinsic electronegativity of each atom and the Coulomb interactions between them. The calculated charges are environment-dependent and change as the geometry of the system changes.

The Born−Mayer repulsive term between atoms i and j reads

$$V_{ij} = A_{ij} \exp\left(-\frac{r_{ij}}{\rho}\right) - C_{ij} r_{ij}^{-6} \qquad (1)$$

where i is an atom of the macrocycle and j is one of the Au atoms. A and C are constants fitted to available ab initio and experimental data,[34] and ρ is 0.296 Å. Specifically, A_{H-Au} = 301.65 kcal mol^{-1}, A_{C-Au} = 15200 kcal mol^{-1}, A_{O-Au} = 14523.44 kcal mol^{-1}, A_{N-Au} = 9229.84 kcal mol^{-1}, C_{H-Au} =

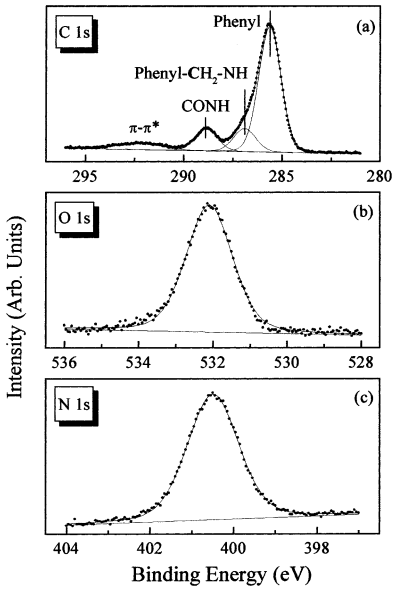

Figure 3. XPS spectra of the (a) C 1s, (b) O 1s, and (c) N 1s core levels from benzylic amide macrocycle multilayers adsorbed on Au(111). Raw data (• •) and fit to the experimental data (——).

0.00 kcal mol^{-1}, $C_{C(sp3)-Au}$ = 990 kcal mol^{-1}, $C_{C(sp2)-Au}$ = 750 kcal mol^{-1}, C_{O-Au} = 435 kcal mol^{-1}, and C_{N-Au} = 276 kcal mol^{-1}.

4. Results and Discussion

4.1. X-ray Photoelectron Spectroscopy. Figure 3 shows XPS spectra of the C 1s, N 1s, and O 1s core levels from multilayers of the benzylic amide macrocycle deposited on Au(111). The film thickness is such that any interfacial interaction with the substrate is obscured, to the extent that the Au $4f_{7/2}$ signal is attenuated to within ~10% of the value typical of clean Au(111), and hence we can consider the photoemission features observed as being representative of a bulklike solid-state sample. Stability checks of the macrocycle to the X-ray beam and secondary electrons produced by photoemission in the underlying metal, performed by monitoring the line shape and relative intensity of the C 1s, N 1s, and O 1s core levels as a function of irradiation time, showed no evidence of charging effects or structural degradation.

In Figure 3a, the main C 1s photoemission is attributed to the phenyl rings with broadening toward higher binding energies due to contributions from the most electron deficient carbon atoms bonded to electronegative nitrogen and oxygen atoms in the amide function and the neighboring aliphatic group. Spectral analysis included a linear background subtraction and peak separation using a mixed Gaussian−Lorentzian function, in a least-squares curve-fitting program (Winspec) developed in our laboratory.[35] While rigorously there are eight chemically distinct carbon environments in the macrocycle shown in Figure 2a, in practice XPS may not distinguish between the six types of phenyl ring carbon. Hence, the decomposition procedure consists of fitting a minimum number of peaks consistent with the raw data and the molecular structure of the adsorbate with the simplification of assuming equivalent aromatic carbon atoms. Figure 3a illustrates a fit to the experimental data (constrained by the theoretical intensity ratio) assuming a molecule with three distinct chemically shifted C 1s core level emissions, occurring at 285.6, 286.9, and 288.9 eV, assigned to the aromatic, aliphatic, and carbonyl components with a shake-up structure

TABLE 1: Core Level Binding Energy (BE) Positions and fwhm for Benzylic Amide Macrocycle Adsorbed at Multilayer and Monolayer Coverage on Au(111)

peak	assignment	BE (eV)	fwhm (eV)	assignment	BE (eV)	fwhm (eV)
C 1s	phenyl	285.6	1.3	phenyl	284.7	1.3
	CH_2	286.9	1.3	CH_2	286.0	1.2
	CONH	288.9	1.5	$CONH^1$	287.3	1.2
				$CONH^2$	288.2	1.1
	$\pi \rightarrow \pi^*$	292.3	2.6	$\pi \rightarrow \pi^*$	293.4	2.8
N 1s	NH	400.5	1.5	NH	399.7	1.3
O 1s	C═O	532.1	1.5	C═O	532.1	1.7
				Au−O	531.2	1.1

associated with π to π^* transitions of the phenyl rings located at 292.3 eV. Peak energy positions and fwhm are given in Table 1. The 1.3 eV binding energy shift relative to benzene (284.3 eV[36]) is understandable given that 33% of the phenyl ring carbons are bonded to CH_2NH or NHCO moieties which themselves display C 1s binding energies well within the range reported in the literature.[22,37]

The experimentally determined X-ray crystal structure, shown schematically in Figure 2a, indicates that in the solid state the benzylic amide macrocycle adopts a staggered, stacked chairlike configuration.[18] Each of the N−H and C═O bonds are directed toward the next nearest molecule above or below to facilitate intermolecular hydrogen bonding (Figure 2a, side view). The N 1s and O 1s regions shown in Figure 3b,c are best described by singlet peaks at 400.5 and 532.1 eV, respectively, consistent with the existence of only one type of nitrogen and oxygen atom environment in the multilayer sample as expected based on the X-ray diffraction data. Interestingly, the O 1s binding energy is in excellent agreement with that reported for the structurally similar $C_6H_5CONH_2$ (532.2 eV) while the N 1s photoemission is chemically shifted by 1 eV to higher binding energy relative to this reference compound (399.5 eV).[22] Presumably, this is a consequence of additional bonding to the CH_2 group, for example the N 1s binding energy reported for cysteine where the NH group is attached to a CH_2 unit is 400.0 eV, and perhaps, to a lesser extent, involvement in intermolecular hydrogen bonding interactions.[37]

The atomic percentage (±0.5%) ratio of carbon, nitrogen and oxygen, was calculated by integration of the areas of the C 1s, N 1s and O 1s peaks after application of a linear background subtraction and correction for atomic sensitivity factors including analyzer transmission.[35] The weak $\pi-\pi^*$ shake-up transition peak included in the curve fitting routine was also considered in the calculation of the relative elemental concentrations.[38] Quantification yields a carbon:nitrogen:oxygen ratio of 8.0:0.97:0.89 which compares favorably with the expected 8:1:1 stoichiometry. Hence, the composition of the thick film indicates the presence of intact molecular species demonstrating that the macrocycle sublimes in UHV without substantial degradation.

To gain insights into the nature of the bonding between the macrocycle and the substrate, we have also characterized a low surface coverage film deposited on Au(111). The carbon coverage can be estimated by comparing the C 1s to Au $4f_{7/2}$ ratio with that measured from a film of known carbon atomic density. Gas-phase chemisorption of mercaptoethanoic acid ($HSCH_2COOH$) to saturation coverage on Au(111) results in a saturation coverage of 0.66 monolayers (ML) of carbon.[20] Ignoring differential attenuation of the carbon and Au signals by the different nature of the monolayers, which should be small at the high outgoing kinetic energies utilized, the corresponding carbon coverage for benzylic amide macrocycle displayed in Figure 4 is 1 ML.

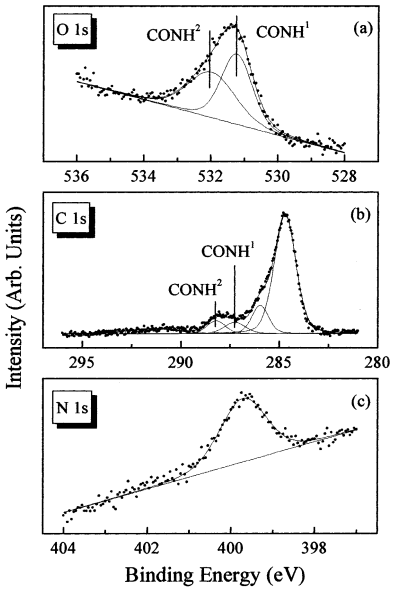

Figure 4. XPS spectra of the (a) O 1s, (b) C 1s, and (c) N 1s core levels from benzylic amide macrocycle at 1 ML carbon coverage adsorbed on Au(111). Raw data (• •) and fit to the experimental data (−−).

At a glance, the C 1s, N 1s, and O 1s spectra presented in Figure 4 do not show significant modifications upon comparison with the thick film previously discussed, with the exception of a shift to lower binding energies for all the peaks under consideration, due to screening by the metal surface. However, closer inspection reveals asymmetry in the O 1s peak line shape and a subtle change in the C 1s photoemission region associated with the amide function. Decomposition of the raw data suggests that the O 1s signal in Figure 4a is composed of two peaks occurring at 531.2 and 532.1 eV with a relative intensity ratio of ∼1:1, and a full width at half-maximum (fwhm) of 1.1 and 1.7 eV, respectively. Comparison with literature values for atomically chemisorbed oxygen and oxide (529.3−530.1 eV) on Au(111) suggests that the low binding energy component is an interfacial Au−O species while the broader higher binding energy peak is consistent with oxygen bound in an organic matrix.[22,39−41] Our data support the formation of two Au−O bonds per macrocyclic ring. In a HREELS study, Fustin et al. have reported chemisorption of a benzylic amide [2]catenane made by two interlocked macrocycles, via two carbonyls on Au(111).[42,43] Given the difference in the solid-state X-ray structures of the two molecules and the fact that most of the hydrogen bonding is intramolecular in the [2]catenane, a difference in bonding configuration is not unexpected.[18,44]

The existence of a new oxygen species is supported by the attenuation of the previously assigned highest binding energy C 1s component. In fact, the carbonyl contribution splits into two peaks at 287.3 and 288.2 eV (intensity ratio = 1:1), denoted as $CONH^1$ and $CONH^2$, respectively, in Figure 4b. Appearance of the additional C 1s species is reasonably assigned to carbonyl groups involved in Au−O bonding in light of the O 1s data. The persistence of the $\pi-\pi^*$ shake-up transition at 293.4 eV indicates that interfacial bonding does not disrupt the electron conjugation of the phenyl rings; hence, any interaction between the surface and the aromatic groups is weak. Chemisorption of the oxygen atom would of course give rise to charge redistribution in the amide function, and in particular, alter the amount of electronic charge contributed to the C═O bond. The location of the O 1s interfacial peak (negatively shifted relative to nonchemisorbed oxygen) should be expected if electron density from substrate atoms is transferred to oxygen atoms of the carbonyl group. A similar shift to lower binding energies is observed in the case of carboxylic acid bonding with Cu atoms where the charge residing on the metal is +1.[45] In contrast, the absence of an interfacial component in the N 1s core level, which consists of a singlet at 399.7 eV (Figure 4c), suggests that the occurrence of oxygen chemisorption has minor consequences for the nitrogen heteroatom in terms of electronic structure. This is hardly surprising given that the effect is tertiary and will be substantially dampened by the carbonyl carbon atom as evidenced by its binding energy shift. Similarly, an STM study of the [2]catenane adsorbed on highly oriented pyrolytic graphite found that the bonding interaction is driven by electrostatic attraction of the carbonyl groups and the substrate.[46] It is also tempting to speculate that carbonyl group chemisorption sterically hinders the neighboring NH moiety from reacting with the Au surface.

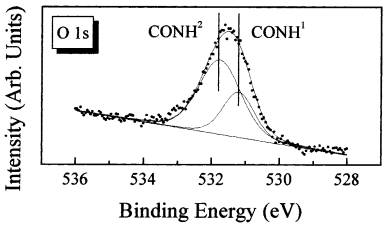

Figure 5. XPS spectra of the O 1s core level from benzylic amide macrocycle at 1.7 ML carbon coverage adsorbed on Au(111). Raw data (• •) and fit to the experimental data (−−).

As additional proof that the 531.2 eV peak is due to Au−O species, the O 1s photoemission from a slightly higher coverage (1.7 ML of carbon estimated as described above) is shown in Figure 5. We would predict that, as the film thickness increases, photoemission from species involved in adsorbate−substrate bonding should be attenuated by the second and subsequent overlayers. As a result, the contribution of the low binding energy Au−O component in Figure 5 is reduced to ∼25%, testifying to its interfacial nature. The nonchemisorbed oxygen component is observed at lower binding energies (531.7 eV).

4.2. High-Resolution Electron Energy Loss Spectroscopy. HREELS data collected in both specular and off-specular scattering geometries from a monolayer coverage of benzylic amide macrocycle adsorbed on Au(111) are shown in Figure 6. The spectra contain the vibrational bands expected upon comparison with solid-state infrared data and a previous HREELS study of a benzylic amide [2]catenane adsorbed on Au(111).[42,47] The prominent vibrational peak observed at 740 cm^{-1} is unambiguously assigned to out-of-plane C−H deformations (γ_{CH}) characteristic of the phenyl rings.[48,49] The corresponding C−H in-plane stretching (ν_{CH}) is identified as the highest energy loss at 2920 cm^{-1} and includes contributions from the aliphatic groups. Given that benzene desorbs from Au(111) above 200 K,[50,51] the presence of the γ_{CH} and ν_{CH} features is particularly relevant as it indicates the intact state of the macrocycle upon sublimation and subsequent adsorption in agreement with the present XPS data. In general, the complex group of unresolved low intensity bands extending from 800 to 1600 cm^{-1} originates from C−H in-plane bending, ring breathing and stretching, amide group deformation, and C−N stretching vibrations with the C═O stretching mode (ν_{CO}) apparent at 1685 cm^{-1}. Finally, the intense energy loss superimposed on the tailing elastic peak at 470 cm^{-1} can be attributed to Au−O stretching (ν_{AuO}) due to chemisorp-

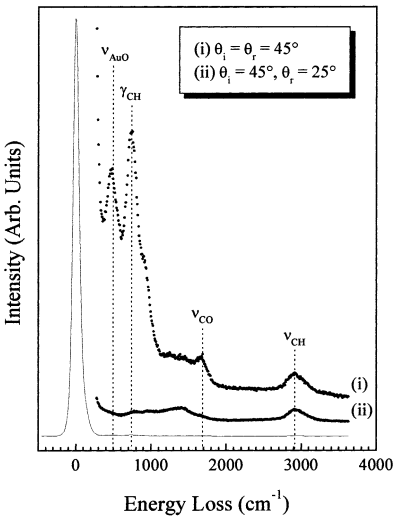

Figure 6. HREELS spectra collected in specular ($\theta_i = \theta_r = 45°$) and off-specular ($\theta_i = 45°$, $\theta_r = 25°$) scattering geometries at a primary beam energy of 6.0 eV from a monolayer film of benzylic amide macrocycle adsorbed on Au(111). Scaling factor = 200.

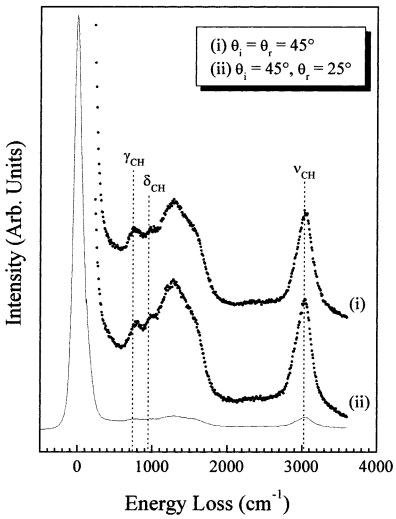

Figure 7. HREELS spectra collected in specular ($\theta_i = \theta_r = 45°$) and off-specular ($\theta_i = 45°$, $\theta_r = 25°$) scattering geometries at a primary beam energy of 6.0 eV from a multilayer film of benzylic amide macrocycle adsorbed on Au(111). Scaling factor = 10.

tion of the macrocycle on the Au surface via the carbonyl function as already inferred from XPS results. Similarly, HREELS studies of formic acid and [2]catenane adsorption on Au(111), report the occurrence of a Au−O stretching vibration at 480 and 484 cm^{-1}, respectively.[42,52,53]

The adsorption geometry of the macrocycle and hence additional information on the nature of surface chemical bonding was obtained by performing off-specular scattering studies and utilizing the metal surface dipole selection rule (MSSR). The selection rule in HREELS applies to specular (dipole) scattering of electrons from molecules adsorbed on a metal surface which effectively screens dynamic dipole moments oriented parallel to the surface such that only those vibrations with a component of the dipole moment change normal to the surface may be observed.[54]

In-plane C−H stretching (ν_{C-H}) has its dipole moment change in the plane of the phenyl ring and hence for an aromatic group oriented perpendicular to the surface it will be strongly excited in the specular scattering geometry. For a molecule with the plane of the ring parallel to the surface, the C−H stretching should have weak intensity (due to nondipolar impact scattering). In contrast, out-of-plane C−H deformation (γ_{C-H}) has a dipole moment perpendicular to the plane of the ring. Hence, this band should be of maximum intensity for a flat-lying molecule and should have low intensity when the plane of the ring is perpendicular to the Au(111) surface. The fact that the ν_{CH} peak at 2920 cm^{-1} is largely due to impact scattering is evidenced by the small change in intensity in moving from specular to off-specular scattering geometries. This observation, together with the extremely low intensity of the in-plane modes in the 800−1600 cm^{-1} region due to strong screening by the Au surface of dipole scattering excitation of these modes, means that we can explicitly eliminate an upright adsorption geometry of the phenyl rings. The data also exclude a geometry in which the phenyl rings are strongly tilted toward the surface normal. Moreover, this is consistent with the relatively large dynamic dipole moment perpendicular to the surface for the γ_{CH} vibration at 740 cm^{-1}, which is clearly the dominant band in the specular spectrum. Off-specular measurements reduce the excitation of this vibration, thus satisfying the dipole selection rule and pointing to an essentially flat-lying orientation of the adsorbed macrocycle. It should also be noted that the fwhm of the elastic peak for the monolayer specular spectrum was typically 12 meV which can be attributed to the highly ordered nature of the film and the relatively narrow distribution of dipolar losses.

A similar application of the dipole selection rule can be used to assess the behavior of the Au−O and C═O stretching vibrations. The ν_{AuO} energy loss displays a strong normal dipole component as evidenced by a sharp intensity decrease in off-specular scattering geometry precluding a bonding configuration with the Au−O bond strongly tilted toward the Au(111) surface. The same is true in the case of the ν_{CO} mode, implying that the C−O bonds are also oriented largely perpendicular with respect to the surface plane.

The HREELS data characteristic of a high coverage, multilayer film shown in Figure 7 is quite different from the monolayer coverage specular spectrum. Specifically, the disappearance of the Au−O stretching vibration affirms that it is indeed an interfacial species arising from chemisorption of the macrocycle on the Au surface. In addition, out-of-plane and in-plane modes of similar intensity are observed and there is negligible difference between specular and off-specular data. The increase in the diffuse scattering properties of the sample are attributed to the absence of a preferred orientation of the phenyl rings in the multilayers and a concomitant decrease in film order reflected by an increase in the elastic peak fwhm to 21 meV.

4.3. Simulation of the Adsorption. The analysis of the spectroscopic data shows that (i) the macrocycle binds to the Au surface with two carbonyls and (ii) its phenyl groups adopt a nearly flat conformation. To obtain more detailed information, five test systems, characterized by different macrocycle coverage of the Au (111) surface, were set up using periodic boundary conditions and were subjected to "simulated annealing" calculations starting from 700 K down to 300 K, see Figure 8. They range from loosely to densely packed macrocycles and the calculations show that they vary greatly for the Au−macrocycle and macrocycle−macrocycle interactions. Table 2 (see also Figure 9) shows both the calculated energies and the angles formed by the phenyls with the Au surface.

The interplay between macrocycle−macrocycle and macrocycle−Au interactions is rather evident. On one hand, the macrocycle−Au interaction decreases linearly with the area of

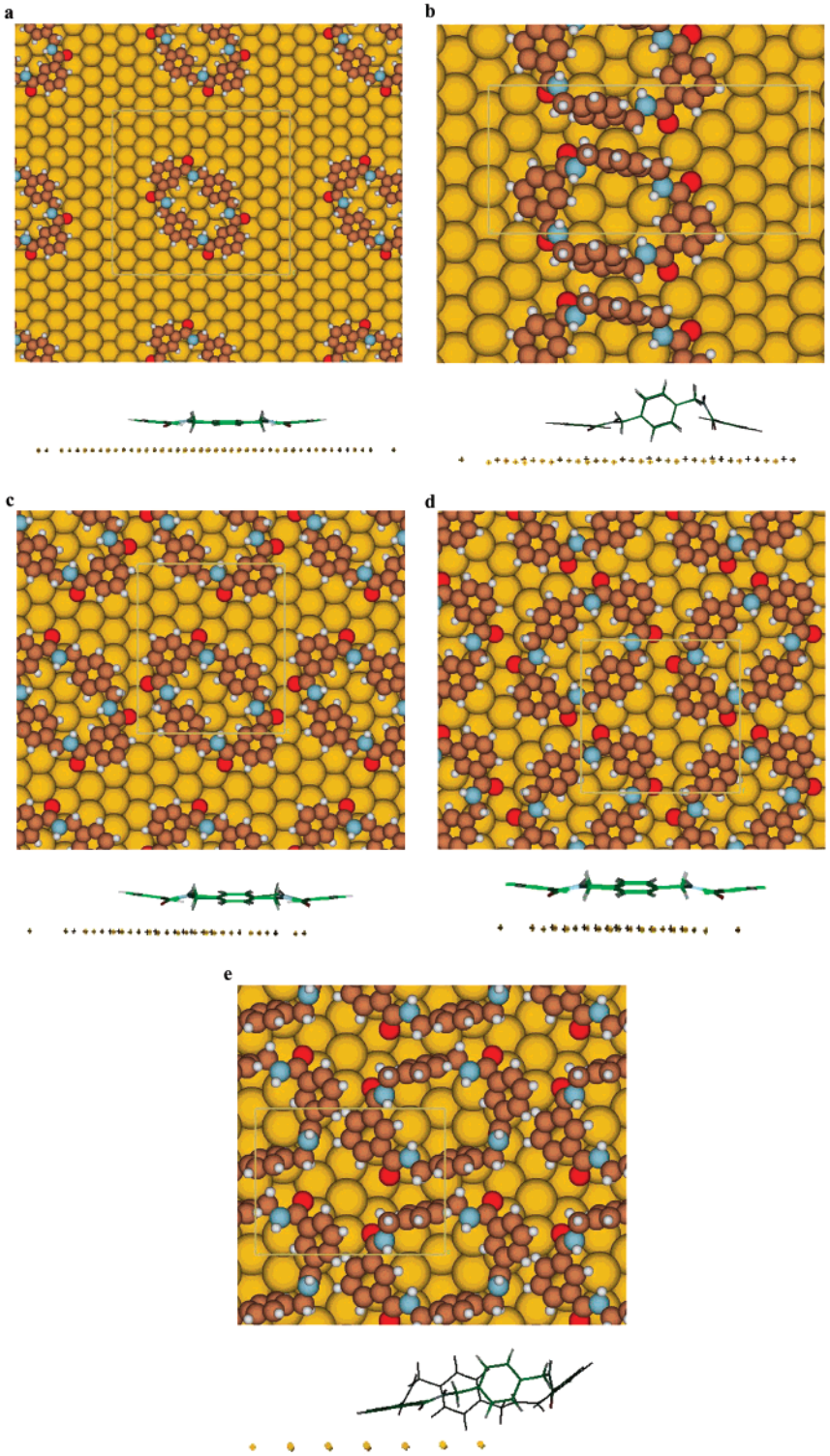

Figure 8. Top and side view of the structures of the macrocycle on Au(111) resulting from simulated annealing: (a) 5 × 8 Au cell, (b) 5 × 4 Au cell, (c) 3 × 6 Au cell, (d) 3 × 5 Au cell, (e) 3 × 4 Au cell. The square shows the cell used for the periodic boundary conditions.

the Au surface cell. The larger the cell area the greater is the interaction so that crowding of the macrocycles affects their ability to bind to the Au surface. On the other hand, the macrocycle-macrocycle interactions first increase with the amount of packing and then decrease or even become destabilized. In fact, the small macrocycle−macrocycle interactions of the Figure 8c,e structures arise from the interference between binding and repulsive energy terms and are therefore qualitatively different from the similar value of the nearly isolated macrocycle of Figure 8a.

Figure 8d shows the most stable structure of the five considered here. Its large stability arises from a combination of binding macrocycle−macrocycle and macrocycle−Au interactions. The phenyls form small angles with the Au surface in agreement with the analysis of the HREELS data. In Figure 8a, the nearly isolated macrocycle possesses a more stabilizing macrocycle−Au interaction than that in Figure 8d, but loses most of the macrocycle-macrocycle stabilization. For this configuration, as well, the phenyls sit nearly flat on the Au surface. The denser packing shown in Figure 8b,c, and e

TABLE 2: Calculated Energies, kcal mol^{-1}, and Angles Formed by the Phenyls with the Au Surface by the Five Systems Investigated in This Work (Dimensions of the Surface Unit Cell in Angstroms)

unit cell[a]	unit cell size	$E_{mac-mac}$	E_{Au-mac}	E_{ads}	ring 1	ring 2	ring 3	ring 4
5 × 8	24.94 × 23.04	−2.88	−106.07	−108.95	5.36	5.03	5.24	4.05
5 × 4	24.94 × 11.52	−17.28	−69.18	−86.46	12.86	65.80	82.00	3.79
3 × 6	14.96 × 17.28	−8.56	−87.11	−95.85	6.43	12.56	12.36	7.73
3 × 5	14.96 × 14.40	−28.06	−83.82	−111.88	6.04	13.98	13.87	5.89
3 × 4	14.96 × 11.52	5.74	−54.76	−49.02	9.83	75.12	80.95	36.98

[a] See Figure 9.

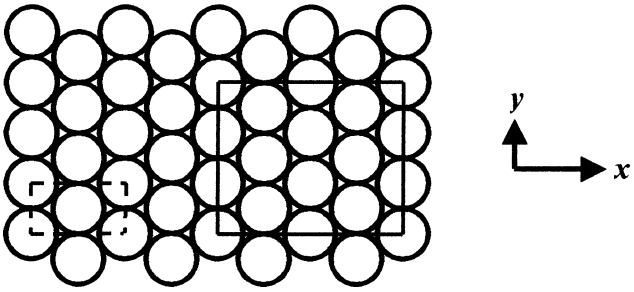

Figure 9. Schematic illustration of the Au(111) unit cells on which the macrocycle was deposited in the calculations. The box on the left (dashed lines) is repeated, in the x and y directions, to form the various cells. Here the unit cell is 2 × 3.

TABLE 3: Oxygen−Gold nearest Neighbors Distances, Angstroms, and Charges in Brackets: In the Isolated Macrocycle, the Oxygen Charge Is −0.491[a]

5 × 8 cell	Au_1	Au_2	Au_3	Au_4
O_1 (−0.558)	2.61 (0.137)	2.68 (0.125)	3.11 (0.105)	3.50 (0.073)
O_2 (−0.559)	2.72 (0.118)	2.77 (0.122)	2.80 (0.120)	3.91 (0.072)
O_3 (−0.559)	2.70 (0.125)	2.72 (0.116)	2.86 (0.116)	3.81 (0.078)
O_4 (−0.558)	2.58 (0.139)	2.71 (0.122)	3.21 (0.099)	3.41 (0.080)
5 × 4 cell	Au_1	Au_2	Au_3	Au_4
O_1 (−0.578)	2.66 (0.113)	2.91 (0.073)	3.27 (0.082)	3.61 (0.101)
O_2 (−0.558)	2.49 (0.131)	3.06 (0.121)	3.36 (0.078)	3.50 (0.184)
O_3 (−0.568)	2.59 (0.136)	2.69 (0.162)	3.02 (0.096)	3.59 (0.086)
O_4 (−0.573)	2.58 (0.125)	2.73 (0.077)	3.14 (0.184)	3.49 (0.066)
3 × 6 cell	Au_1	Au_2	Au_3	Au_4
O_1 (−0.561)	2.55 (0.135)	2.63 (0.177)	3.15 (0.087)	3.40 (0.083)
O_2 (−0.573)	2.59 (0.103)	2.70 (0.116)	2.97 (0.211)	3.61 (0.090)
O_3 (−0.573)	2.67 (0.115)	2.74 (0.089)	2.78 (0.211)	3.94 (0.130)
O_4 (−0.561)	2.57 (0.166)	2.62 (0.133)	3.15 (0.100)	3.40 (0.067)
3 × 5 cell	Au_1	Au_2	Au_3	Au_4
O_1 (−0.561)	2.65 (0.128)	2.65 (0.221)	2.85 (0.084)	3.74 (0.139)
O_2 (−0.576)	2.53 (0.125)	2.70 (0.214)	3.06 (0.110)	3.50 (0.089)
O_3 (−0.576)	2.50 (0.121)	2.75 (0.214)	3.24 (0.119)	3.36 (0.092)
O_4 (−0.561)	2.65 (0.106)	2.69 (0.124)	2.79 (0.221)	3.78 (0.083)
3 × 4 cell	Au_1	Au_2	Au_3	Au_4
O_1 (−0.574)	2.59 (0.150)	2.77 (0.108)	2.93 (0.126)	3.72 (0.059)
O_2 (−0.563)	2.79 (0.084)	2.80 (0.130)	2.96 (0.101)	3.88 (0.065)
O_3 (−0.566)	2.61 (0.112)	3.02 (0.066)	3.46 (0.077)	3.49 (0.085)
O_4 (−0.593)	2.62 (0.069)	3.19 (0.093)	3.20 (0.057)	3.87 (0.071)

[a] In Figure 8 the five cells are labeled from a− e.

modifies the macrocycle conformation whose phenyls are no longer lying flat on the Au(111) surface and therefore do not match the HREELS analysis. These structures are also less stable than those discussed above and will therefore not be considered further.

The small energy difference between the structures of Figure 8a,d may not allow one to chose which one is actually favored experimentally. Table 3 shows the O−Au nearest neighbor distances together with the charges obtained by the Qeq method. The qualitative picture emerging from the HREELS measurements supported by the quantitative XPS result of two oxygens bound to the Au surface is replaced by a number of distances that do not help to distinguish whether a pair of oxygens is more strongly linked to the surface than the other pair. Examination of the oxygen charges, however, shows that in the more stable structure of Figure 8d the oxygens have higher charges than in the case of the structure of Figure 8a. Satisfactorily, they also split into two pairs. On the contrary, the structure of Figure 8a is characterized by similar charges on all the oxygen atoms. It is concluded that the configuration of Figure 8d corresponds best to the experimental findings both on the basis of its energy and because it reproduces the nearly flat position of the phenyls and the existence of two pairs of diversely adsorbed oxygens. Importantly, such pairs form through the presence of macrocycle−macrocycle interactions and the oxygen chemical shifts can become a fingerprint for the amount of surface coverage.

5. Conclusions

We have presented XPS and HREELS characterization of the adsorption of the prototypical benzylic amide macrocycle on Au(111). Our results show that the initial stages of film growth proceed via chemisorption of the amide functions on the metal surface with the bonding interaction localized in two carbonyl groups. The observation that the out-of-plane phenyl ring deformation mode is dipole active and the dynamic dipole of this mode is perpendicular to the surface made us assign a flat-lying adsorption geometry at monolayer coverage. Both assignments were corroborated by molecular mechanics and charge equilibration calculations which showed that the difference in behavior of two carbonyls with respect to the other two originates in macrocycle−macrocycle interactions.

Acknowledgment. The authors gratefully acknowledge C. De Nadaï and C.-A. Fustin for invaluable discussions. This work was carried out within the DRUM and ENBAC networks supported by the European Commision, TMR contracts FMRX-CT97-0097 and FMRX-CT96-0059, respectively, and has also been partially funded by the Belgian Inter-University Program on "Reduced Dimensionality Systems" PAI/IUAP 4/10 initiated by the Belgian Office for Scientific, Technological and Cultural Affairs.

References and Notes

(1) Anelli, P.-L.; Spencer, N.; Stoddart, J. F. *J. Am. Chem. Soc.* **1991**, *113*, 5131.

(2) Bissell, R. A.; Córdova, E.; Kaifer, A. E.; Stoddart, J. F. *Nature* **1994**, *369*, 133.

(3) Collin, J.-P.; Gavinã, P.; Sauvage, J.-P. *New J. Chem.* **1996**, *21*, 525.

(4) Lane, A. S.; Leigh, D. A.; Murphy, A. *J. Am. Chem. Soc.* **1997**, *119*, 11092.

(5) Murakami, H.; Kawabuchi, A.; Kotoo, K.; Kunitake, M.; Nakashima, N. *J. Am. Chem. Soc.*, **1997**, *119*, 7605.

(6) Kelly, T. R.; Bowyer, M. C.; Vijaya Bhaskar, K.; Bebbington, D.; Garcia, A.; Lang, F.; Kim, M. H.; Jette, M. P. *J. Am. Chem. Soc.* **1994**, *116*, 3657.

(7) Kelly, T. R.; Tellitu, I.; Sestelo, J. P. *Angew. Chem., Int. Ed. Engl.* **1997**, *36*, 1866.

(8) Davis, A. P. *Angew. Chem., Int. Ed. Engl.* **1998**, *37*, 909.

(9) Bedard, T. C.; Moore, J. S. *J. Am. Chem. Soc.* **1995**, *117*, 10662.

(10) Kelly, T. R.; De Silva, H.; Silva, R. A. *Nature* **1999**, *401*, 150.

(11) Koumura, N.; R. W. Zijlstra, J.; van Delden, R. A.; Harada, N.; Feringa, B. L. *Nature* **1999**, *401*, 152.

(12) Feynman, R. P. In *Miniaturization*; Gilbert, H. D., Ed.; Reinhold: New York, 1961.

(13) Mislow, K. *Chemtracts: Org. Chem.* **1989**, *2*, 151.

(14) Balzani, V.; Gómez-López, M.; Stoddart, J. F. *Acc. Chem. Res.* **1998**, *31*, 405.

(15) Sauvage, J.-P. *Acc. Chem. Res.* **1998**, *31*, 611.

(16) Gimzewski, J. *Phys. World* **1998**, *11*, 29.

(17) Sauvage, J.-P., Dietrich-Buchecker, C. O. Eds. *Molecular Catenanes, Rotaxanes and Knots*; Wiley-VCH: Weiheim, 1999.

(18) Clarkson, G. J.; Lacy, S.; Leigh, D. A.; Nepogodiev, S.; Slawin, A. M. Z.; Wong, J. Y. K. In preparation.

(19) Johnston, A. G.; Leigh, D. A.; Murphy, A.; Smart, J. P.; Deegan, M. D. *J. Am. Chem. Soc.* **1996**, *118*, 10662.

(20) Whelan, C. M.; Barnes, C. J.; Pireaux, J.-J. In preparation.

(21) Thiry, P. A.; Pireaux, J.-J.; Caudano, R. *Phys. Mag.* **1981**, *4*, 35.

(22) Moulder, J. F.; Stickle, W. F.; Sobol, P. E.; Bomben, K. D. *Handbook of Photoelectron Spectroscopy*; Perkin-Elmer Corporation, Physical Electronics Division: Eden Prairie, MN 55344, 1992.

(23) Bermudez, V.; Capron, N.; Gase, T.; Gatti, F. G.; Kajzar, F.; Leigh, D. A.; Zerbetto, F.; Zhang, S. *Nature* **2000**, *406*, 608.

(24) Fustin, C.-A.; Leigh, D. A.; Rudolf, P.; Timpel, D.; Zerbetto, F. *Chem. Phys. Chem.* **2000**, *1*, 97.

(25) Leigh, D. A.; Parker, S. F.; Timpel, D.; Zerbetto, F. *J. Chem. Phys.* **2001**, *114*, 5006.

(26) Allinger, N. L.; Yuh, Y. H.; Lii, J.-H. *J. Am. Chem. Soc.* **1989**, *111*, 8551.

(27) Lii, J.-H.; Allinger, N. L. *J. Am. Chem. Soc.* **1989**, *111*, 8566.

(28) Lii, J.-H.; Allinger, N. L. *J. Am. Chem. Soc.* **1989**, *111*, 8576.

(29) Ponder, J.; Richards, F. *J. Comput. Chem.* **1986**, *8*, 1016.

(30) Kundrot, C.; Ponder, J.; Richards, F. *J. Comput. Chem.* **1991**, *12*, 402.

(31) Dudek, M.; Ponder, J. *J. Comput. Chem.* **1995**, *16*, 791.

(32) Ercolessi, F.; Parrinello, M.; Tosatti, E. *Phys. Mag. A* **1988**, *58*, 213.

(33) Rappe, A. K.; Goddard, W. A., III. *J. Phys. Chem.* **1991**, *95*, 3358.

(34) Baxter, R.; Zerbetto, F. In preparation.

(35) Quantification and peak analysis performed using the curve-fitting routines provided by Scienta showed agreement with Winspec results within ±5% allowing intercomparison of data and trends.

(36) Riga, J.; Pireaux, J.-J.; Verbist, J. *Mol. Phys.* **1977**, *34*, 131.

(37) Beamson, G.; Briggs, D. *High-Resolution XPS of Organic Polymers*; The Scienta ESCA300 Database; John Wiley & Sons Ltd.: Chichester 1992.

(38) The $\pi-\pi^*$ shake-up intensity was included in the phenyl peak. For precise analysis, a carbonyl carbon shake-up should also be included. However, as its intensity is predicted to be low (<10%), we neglected its contribution.

(39) Saliba, N.; Parker, D. H.; Koel, B. E. *Surf. Sci.* **1998**, *410*, 270.

(40) Krozer, A.; Rodah, M. *J. Vac. Sci. Technol. A* **1997**, *15*, 1704.

(41) Takamatsu, S.; Ishi-i, M.; Imagawa, M.; Kinbara, H.; Kibuta, T.; Fukushima, T. *Catal. Soc. Jpn.* **1992**, *34*, 126.

(42) Fustin, C. A.; Rudolf, P.; Taminiaux, A. F.; Zerbetto, F.; Leigh, D. A.; Caudano, R. *Thin Solid Films* **1998**, *327−329*, 321.

(43) Fustin, C. A.; Gouttebaron, R.; Caudano, R.; Rudolf, P.; Leigh, D. A.; Fanti, M.; Krug, A.; Zerbetto, F. Submitted for publication.

(44) Johnston, A. G.; Leigh, D. A.; Pritchard, R. J.; Deegan, M. D. *Angew. Chem., Int. Ed. Engl.* **1995**, *34*, 1209.

(45) Czanderna, A. W.; King, D. E.; Spaulding, D. *J. Vac. Sci. Technol. A* **1991**, *9*, 2607.

(46) Biscarini, F.; Gebauer, W.; Di Domenica, D.; Zamboni, R.; Pascual, J. I.; Leigh, D. A.; Murphy, A.; Tetard, D. *Synth. Met.* **1999**, *102*, 1466.

(47) Whelan, C. M.; Cecchet, F.; Clarkson, G. J.; Leigh, D. A.; Caudano, R.; Rudolf, P. *Surf. Sci.* **2001**, *474*, 71.

(48) Bellamy, L. J. *The Infrared Spectra of Complex Molecules*; Methuen and Co. Ltd.: London, 1966.

(49) Socrates, G. *Infrared Characteristic Group Frequencies*, John Wiley & Sons: Chichester, 1980.

(50) Netzer, F. P. *Langmuir* **1991**, *7*, 2544.

(51) Weiss, K.; Gebert, S.; Wuhn, M.; Wadephol, H.; Woll, C. *J. Vac. Sci. Technol. A* **1998**, *16*, 1017.

(52) Chtaïb, M. Thiry, P. A.; Pireaux, J.-J.; Delrue, J. P.; Caudano, R. *Surf. Sci.* **1985**, *162*, 245.

(53) Chtaïb, M.; Thiry, P. A.; Delrue, J. P.; Pireaux, J.-J.; Caudano, R. *J. Electron Spectrosc. Relat. Phenom.* **1983**, *29*, 293.

(54) Ibach, H.; Mills, D. L. *Electron Energy Loss Spectroscopy and Surface Vibrations*; Academic: London, 1982.